Magnetic Resonance in Medicine 42:963–969 (1999)

Motion Correction With PROPELLER MRI: Application to Head Motion and Free-Breathing Cardiac Imaging

James G. Pipe*

A method for motion correction, involving both data collection and reconstruction, is presented. The PROPELLER MRI method collects data in concentric rectangular strips rotated about the *k*-space origin. The central region of *k*-space is sampled for every strip, which (a) allows one to correct spatial inconsistencies in position, rotation, and phase between strips, (b) allows one to reject data based on a correlation measure indicating through-plane motion, and (c) further decreases motion artifacts through an averaging effect for low spatial frequencies. Results are shown in which PROPELLER MRI is used to correct for bulk motion in head images and respiratory motion in nongated cardiac images. Magn Reson Med 42:963–969, 1999.

Key words: motion correction; cardiac; *k*-space; rotation

Patient motion is known to produce artifacts in MR imaging. These artifacts can arise as a result of tissue displacement during the quiescent period between each data sampling period and the following excitation rf (referred to here as type I artifact), and also as a result of spin phase induced by motion through magnetic field gradients between an excitation rf pulse and the subsequent data sampling period (type II artifact). Many methods have been used to mitigate these motion artifacts; a limited number are discussed in this article.

Center-out imaging methods such as projection-reconstruction (1) and spiral (2,3) MRI have been shown to reduce motion artifacts. This is attributable in part to oversampling of central *k*-space, which reduces artifact in a manner similar to multiple averaging in conventional imaging. Additionally, when data collection begins at the center of *k*-space, in-plane gradient moments are greatly reduced in the central region of *k*-space, minimizing type II artifacts (4).

Another method for motion artifact reduction involves measurement of motion or motion-related phase through extra collected data, referred to as navigator echoes (5). These navigator echoes can be used to correct for bulk motion between phase encodings to reduce type I artifact. Application of navigator echoes is also used with diffusion-weighted MRI to remove linear phase in image space caused by bulk motion (type II artifact) (6). Navigator echoes may also be used to ''throw out'' data collected when there is significant motion, trading longer data collection times for reduced motion artifacts (7).

This work presents a new method of data collection and reconstruction for reducing motion artifact, called Periodically Rotated Overlapping ParallEL Lines with Enhanced Reconstruction (PROPELLER) MRI. The method has the advantages of oversampling at the center of *k*-space and obtains inherent ''navigator'' information, which may be used in ways similar to those discussed above. The latter aspect of PROPELLER MRI permits correction for in-plane displacement and rotation (type I artifacts), image phase due to motion (type II artifacts), and through-plane motion. In this paper, the data collection and reconstruction process are discussed, followed by applications of head motion (bulk rigid body motions) and respiratory motion in cardiac imaging, in which only local motions of the left ventricle are used for correction.

THEORY

The data collection and reconstruction, as outlined in Fig. 1, are explained in detail in the following discussion.

Data Collection

PROPELLER data are collected in *k*-space in N strips, each consisting of L parallel linear trajectories, corresponding to the L lowest frequency phase encoded lines in any Cartesian-based data collection method. A single strip is shown in Fig. 2a. In general, each strip of phase encoded lines can be collected using a variety of methods, either with a single excitation rf pulse and multiple readouts (e.g., turbo-spin-echo or partial echo-planar sequences), or with a series of excitation rf pulses (e.g., fast gradient echo).

The strips are successively rotated in *k*-space by an incremental angle

$$d\alpha = \frac{\pi}{N}, \qquad [1]$$

so that the total data set spans a circle in *k*-space, as illustrated in Fig. 2b. If an effective matrix diameter of M is desired, L and N are chosen so that

$$LN = M\frac{\pi}{2}. \qquad [2]$$

As a result of the overlap between strips, a central circle in *k*-space with diameter L is resampled for every strip. At higher spatial frequencies, the overlap decreases, and peripheral *k*-space values are measured by a single strip.

The above discussion on data collection assumed circular *k*-space coverage (isotropic resolution) and a circular field of view (FOV). Where appropriate, decreasing the FOV in one direction only, while maintaining isotropic resolution, allows one to save time by collecting fewer strips, or fewer lines per strip, than are necessary for a symmetric FOV. The desired result is a set of *k*-space sampling trajectories such as that illustrated in Fig. 3. The

Department of Radiology, Wayne State University, Detroit, Michigan.

*Correspondence to: James Pipe, MRI Department, St. Joseph's Hospital and Medical Center, 350 W. Thomas Road, Phoenix, AZ 85013.

Received 17 March 1999; revised 15 July 1999; accepted 16 July 1999.

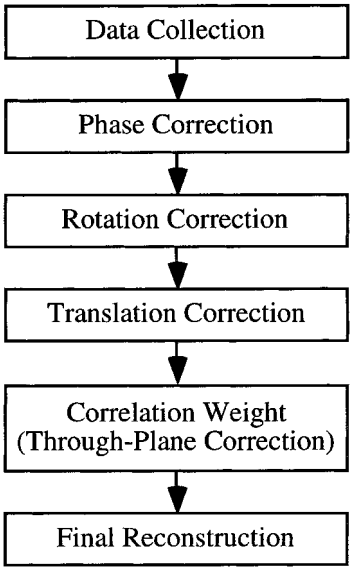

FIG. 1. Diagram of the PROPELLER collection reconstruction process for motion corrected MRI.

resolution, and therefore the extent of coverage, is isotropic; however, the FOV, and therefore the line spacing, varies elliptically. The data matrix is now elliptical, with major and minor axes M_x and M_y (or vice-versa). Using the equation for an ellipse in polar coordinates, the effective matrix M_α for a strip at a given angle α_a is derived as

$$M_\alpha = \left\{\left[\frac{\cos(\alpha_a)}{M_x}\right]^2 + \left[\frac{\sin(\alpha_a)}{M_y}\right]^2\right\}^{-1/2}. \quad [3]$$

The line spacing for a given strip is therefore equal to (M_α resolution)$^{-1}$. The incremented angle given in Eq. [1] is valid only for an isotropic FOV; when strips are widened anisotropically, the angle α_a can be obtained via the equation

$$\alpha_a = \alpha_i + c \sin(2\,\alpha_i), \quad [4]$$

where α_i is the angle for corresponding isotropic acquisition, and c is an empirical "fudge factor" used to make the edges of adjacent strips touch. Typical values of c vary from

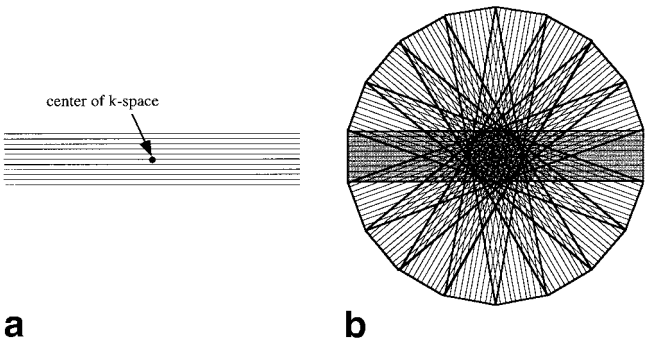

FIG. 2. Illustration of (**a**) a single strip in *k*-space, composed of *L* phase encoded lines corresponding to a full image set with very low resolution in the phase-encoded direction, and (**b**) a complete set of trajectories for a PROPELLER data set, composed of concentric rotated strips.

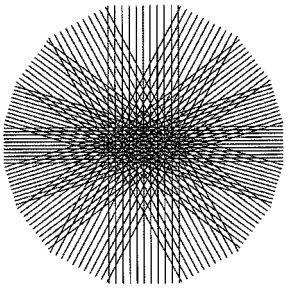

FIG. 3. Illustration of trajectories for an asymmetric FOV ($N = 8$, $L = 11$, $M_x = 40$, $M_y = 80$).

5° to 15°. A more rigorous definition of α_a has not been found.

Phase Correction

A necessary step before combining the data from the strips is make sure that the point of rotation is the center of *k*-space. This is generally not exactly true, due to imperfect gradient balancing along the readout direction and eddy currents. This displacement of the *k*-space center results in a linear phase variation in image space for each of the strips. One can remove all low-frequency spatially varying phase in image space for each strip, simultaneously removing *k*-space translation, as well as eliminating motion-related phase, which varies slowly over the image and may also vary from strip to strip. This approach is illustrated in Fig. 4. Each strip is windowed by a pyramid function (separable triangles), and the resulting phase of these windowed data is removed from the original data in image space. The reason for windowing by a triangular-shaped function is that its Fourier transform, $\mathrm{sinc}^2(x)$, has no negative values, and therefore the low-frequency phase estimation does not contain "artificial" 180° phase shifts (i.e., negative real values) from Gibb's ringing, which should not be removed in the phase correction process. The two-dimensional (2D) FFTs are zero-padded to prevent mixing the positive and negative high spatial frequency information during the phase correction.

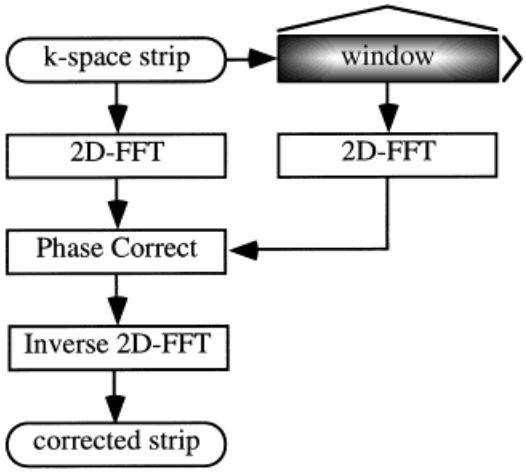

FIG. 4. Diagram of the phase correction process for each strip during PROPELLER reconstruction.

Bulk Rotation Correction

After phase correction of the data, bulk rotation of the object between each strip is estimated and removed. It is well known that rotation of an object in image space produces identical rotations of its Fourier transform in *k*-space, while shifts of an object in image space produce linear phase shifts in the *k*-space data. Thus, if one looks only at the magnitude of *k*-space data, the bulk rotation of an object can be assessed independent of its bulk translation. There are efficient methods of estimating this rotation (8,9); the method presented in this article and used in the applications described below was chosen for its simplicity to implement, rather than for its computational efficiency.

As stated above, there is a circle in the center of *k*-space, *L*/FOV in diameter, that is measured for each strip. A set of Cartesian coordinates that spans this central circle is defined as *R*. The data magnitude M_n of each strip (where *n* is the strip index running from 1 to *N*) inside this circle is gridded onto *R*, and averaged together to form a reference data set in *k*-space M_A with the magnitude-weighted ''average'' rotation. Each M_n is then rotated by a series of angles and gridded onto *R* for each angle. The set of angles spans a user-specified range that covers the expected range of rotations. For each strip, the correlation of M_A and M_n is measured as a function of rotation angle. This correlation should be largest when M_n is rotated to the magnitude-weighted average rotation of M_A. It was found empirically that this correlation is more robust if each datum in M_A and M_n is first multiplied by the square of its distance from the *k*-space origin; this removes the heavy weighting at the *k*-space center due to the concentration of signal energy at low spatial frequencies, and places more emphasis at the edges of *R*, where small rotations produce a larger azimuthal shift.

The correlation, as a function of rotation angle, is then fit to a second-order polynomial, and the peak of the fit polynomial is estimated to be the angle of rotation for the *n*th strip. Once the angles are estimated for each strip, the respective strip coordinates are rotated to match the estimated rotation of the object at the time of data collection. These rotated coordinates are then used in the translation correction and correlation weighting algorithms, as well as in the final reconstruction.

Bulk Translation Correction

Bulk translation is estimated by comparing the data in the central circle with an averaged data set, as done for bulk rotation estimation. In this case, however, the data are kept complex, and an average complex data set D_A is formed on the Cartesian coordinates *R*. If D_A and D_n (the complex data for the *n*th strip contained within the central circle of diameter *L*/FOV) form low-resolution images d_A and d_n, respectively, then the translation for each strip can be found by finding the maximum value of the convolution of d_A* and d_n. This convolution is best performed by first multiplying D_A* by D_n, and taking the Fourier transform of the product. After this Fourier transform is taken, the peak magnitude is found, and a three-point parabolic fit of the magnitudes about that peak in the *x* and *y* directions is performed. The location of the vertex of this parabola is the estimated translation in the *x* and *y* directions, and a corresponding linear phase is removed from the collected data in that strip.

Correlation Weighting

The rotated and translated data are then correlated with each other. Poor correlation between data strips is assumed to correspond to significant through-plane motion, uncorrected in-plane motion (e.g., nonrigid body motion), or some other factor that would create artifacts in the final reconstructed image. The following method allows one to prioritize the data from each strip based on correlation with the average data, and then to weight the data unevenly, according to priority, in areas of strip overlap to minimize the contribution of strips associated with through-plane motion, and other factors.

The data for each strip, after translation correction, are gridded onto *R* within the central circle to form *N* data sets D'_n. From these data, a new average data set D'_A is formed. A correlation measure c_n of each strip is calculated as

$$\chi_n = \left| \int_R D'_A D'^{*}_n \right| . \qquad [5]$$

These *N* correlation values are normalized to span between 0.1 and 1 and are then raised to the power ρ form correlation weights *P*, i.e.,

$$P_n = \left[0.1 + 0.9 \left(\frac{\chi_n - \chi_{\min}}{\chi_{\max} - \chi_{\min}} \right) \right]^{\rho} . \qquad [6]$$

The values of P_n determine relative contributions from overlapping strips during the gridding process described below. The choice of r represents a tradeoff between rejection of bad data (large ρ) and the smoothing effect one gets from oversampling the center of *k*-space (small ρ, resulting in more averaging and less data rejection). In the reconstructed images for this work, $\rho = 2$.

Final Reconstruction

Final reconstruction involves gridding the data, Fourier transforming the result, correcting for signal rolloff from the gridding procedure (10), and taking the real value of the complex result. This last operation is possible because of the phase correction step, and results in better signal to noise ratio (SNR) than is obtained using magnitude images. The gridding is done using rotated coordinates as well as data that are translation and phase-corrected in image space and correlation weighted. Pre-gridding weights are assigned by modifying a previously published sampling density correction method (11). In that method, the weighting for each point is calculated by solving the iteration

$$W_{i+1} = \frac{W_i}{W_i \otimes C} , \qquad [7]$$

where W is the set of pregridding weights in *k*-space, ⊗ denotes the convulation operation, *C* is a convolution function, and *i* is the index of iteration. The rationale for this approach is that as this iteration converges, $W \otimes C$ will approach unity at each sampling location, giving uniform

sampling density at the sampled locations. The modification to this approach is to use the iteration

$$W_{i+1} = \frac{W_i}{(PW_i) \otimes C}, \quad [8]$$

forcing $(PW) \otimes C$ to approach unity, and therefore forcing the weighting function to correct for both sampling density and correlation weighting. For example, if strips with correlation weights 0.9 and 0.6 overlap, the relative weighting function would be roughly 1/1.5 in the area of overlap (assuming otherwise uniform sampling density), and therefore the data would be multiplied by $PW = 0.9/1.5$ and 0.6/1.5, respectively. In practice, initial values of W that solve Eq. [7] are stored, and then used in Eq. [8] for one or two iterations after P has been calculated. These final iterations also correct for changes in the sampling density after each strip is corrected for rotation.

Regional Corrections

The above discussion corrected for rigid body motions over the entire image. For applications such as respiratory motion correction for cardiac imaging, these corrections do a poor job of correcting for local heart motion. A slight modification of the algorithms allows one to select an area of the image (e.g., the left ventricle) in which the rigid body motion assumption is more valid and to base the corrections on the regional bulk motion in that area only. The following method illustrates one way to perform this scheme.

All the data are initially gridded, without correction, onto R, forming N template data sets T_n, which are then Fourier transformed to N low-resolution images t_n. These images are summed to create an average low-resolution image, allowing a user to identify a region of interest (ROI) in which to track motion. Each t_n is multiplied by a tapered mask that removes data outside of the ROI, and transformed back into Fourier space, giving T'_n. Each data set now represents only the contribution to T_n from the signal inside the ROI. The rotation and translation estimations discussed earlier are performed using T'_n, and the estimated motions are removed from the original, unmasked data for the final reconstruction. Correlation weights may be computed using either the masked data T'_n or the full data set, depending on whether poor signal correlation outside of the ROI may indicate poor signal correlation inside of the ROI.

APPLICATION

PROPELLER MRI was implemented on a Siemens Vision scanner. The data were reconstructed using in-house software incorporated into the AVS software platform (Advanced Visual Systems, Waltham, MA) on an UltraSparc 30 workstation (Sun Microsystems, MountainView, CO).

Head Motion

A turbo-spin-echo sequence was modified to collect T_2-weighted PROPELLER data. The sequence had a TR/TE of 3000/100 msec, 230-mm FOV, 4-mm slice thickness, and an effective matrix diameter of 256. Each echo train collected all 24 lines for a single strip, and 17 strips were collected. A conventional turbo-spin-echo sequence was written for comparison, which collected 240 interleaved phase encoding lines over 10 TR, but was otherwise identical to the PROPELLER sequence. For each sequence, two axial data sets were collected; first with no motion, and then with the volunteer moving his head randomly (up to a few cm in all directions) during the entire experiment. The head motion included both in-plane rotation and translation as well as through-plane motion.

Figure 5 shows images from the conventional sequence and the PROPELLER sequences with varying amounts of motion correction. One can appreciate by comparing Fig. 5b,e that PROPELLER data collection without any motion correction reduces motion artifact relative to conventional scanning. This is attributable to the averaging effect one obtains by resampling the center region of k-space N times. With motion correction, the PROPELLER image in Fig. 5i with patient motion approaches the quality of the images with no patient motion.

Respiratory Motion: Free-Breathing Cardiac MRI

A turbo-spin-echo sequence was modified to collect T_2-weighted PROPELLER cardiac data. The sequence used a double-inversion pulse (12) for black blood imaging with an inversion time of 500 msec (double inversion occurred at the R-wave trigger). The electrocardiographic (ECG) gated sequence had a TR/TE of three heartbeats/60 msec, 400-mm FOV, 6-mm slice thickness, frequency-selective fat saturation, and an effective matrix diameter of 256. Each echo train collected all 24 lines for a single strip, and 17 strips were collected. A conventional turbo-spin-echo sequence was written for comparison, which collected 240 interleaved phase encoding lines over 10 TR but was otherwise identical to the PROPELLER sequence. Data were collected twice for each sequence along the short axis of the heart of a normal volunteer for each sequence; first with normal breathing, and then with small shallow breaths in-between data collection and an end-exhalation diaphragm position for each TR (pseudo-breath-hold). Regional motion correction was performed using only a limited FOV around the left ventricle. Rotation corrections were not robust for this application due to the circular symmetry of the left ventricle and were therefore not included in the reconstruction.

Figure 6 shows images from the conventional sequence and the PROPELLER sequences without and with motion correction. As seen in Fig. 5, PROPELLER data collection without any motion correction reduces respiratory motion artifact relative to conventional scanning. With motion correction, the PROPELLER image in Fig. 6f with free breathing approaches the quality of the breath-hold images.

DISCUSSION

PROPELLER MRI, as outlined above, may be implemented with any method that collects data along parallel lines, including standard spin and gradient echo, echo-planar,

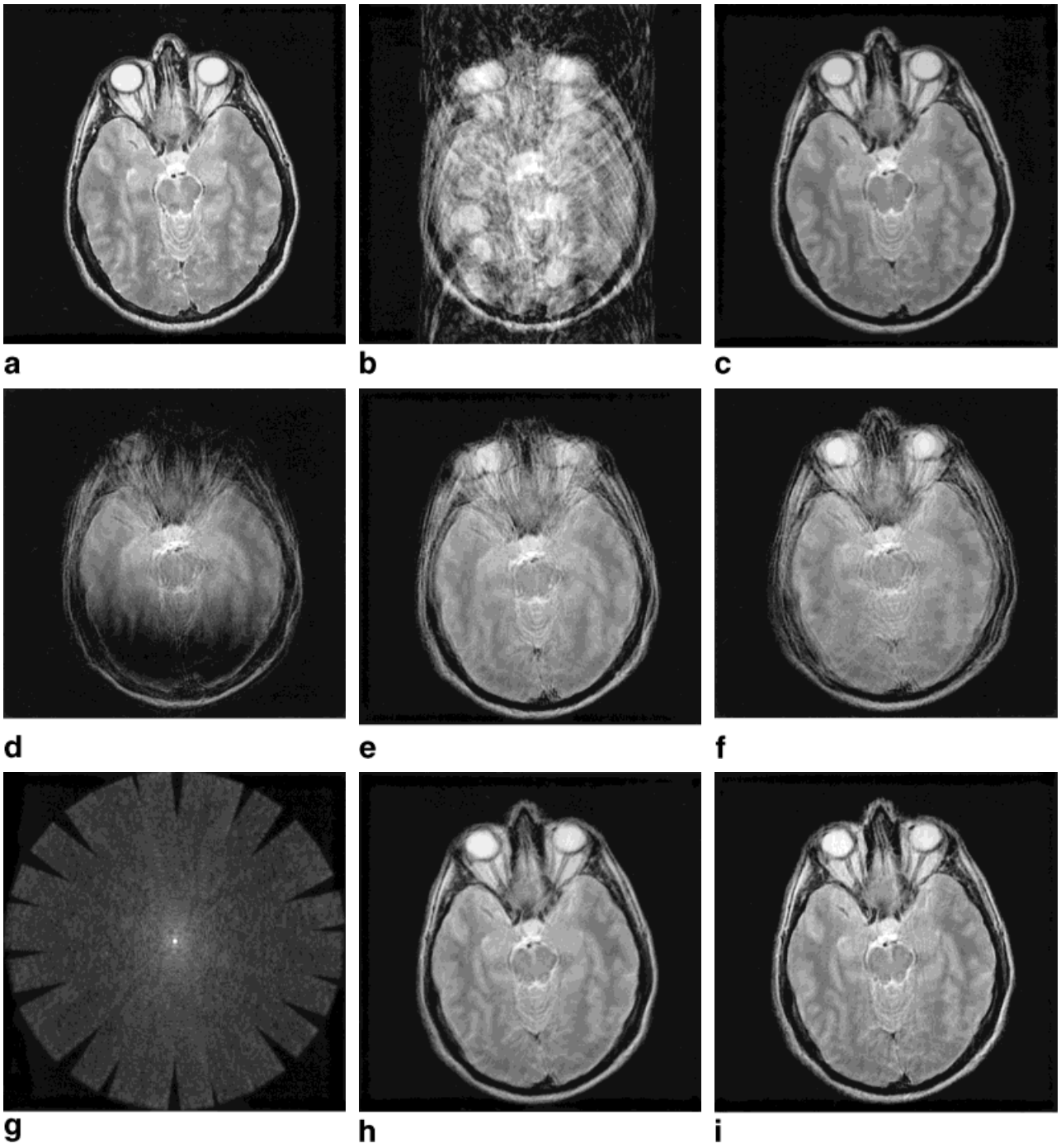

FIG. 5. Axial images of a head with a conventional turbo-spin-echo sequence both without (**a**) and with (**b**) motion, and the PROPELLER sequence both without (**c**) and with (**d–i**) motion. Data for PROPELLER with motion are shown after (**d**) no correction, (**e**) phase correction, (**f,g**) rotation correction (image and *k*-space, respectively), (**h**) shift correction, and (**i**) correlation (through-plane) correction. Magnitude data (**g**) are raised to the 0.2 power for display purposes.

grase, and magnetization prepared turbo-spin-echo and turbo gradient echo sequences. The PROPELLER MRI method is well suited for imaging moving objects, due to its inherent ability to remove some of the in-plane motion, reject some of the artifact from through-plane motion, and its inherent averaging of the remaining data inconsistencies. The collection requires an additional factor of $\pi/2$ imaging time over conventional scans, due to redundant sampling of *k*-space, but the oversampling also results in increased SNR. The ability to use real-valued reconstruction, when appropriate, further increases SNR.

It is expected that PROPELLER MRI will also work well for multishot diffusion MRI, similar to that discussed by Butts et al. (13). As long as the motion-related phase from the diffusion gradients is slowly varying, the data from individual strips may be added together with minimal

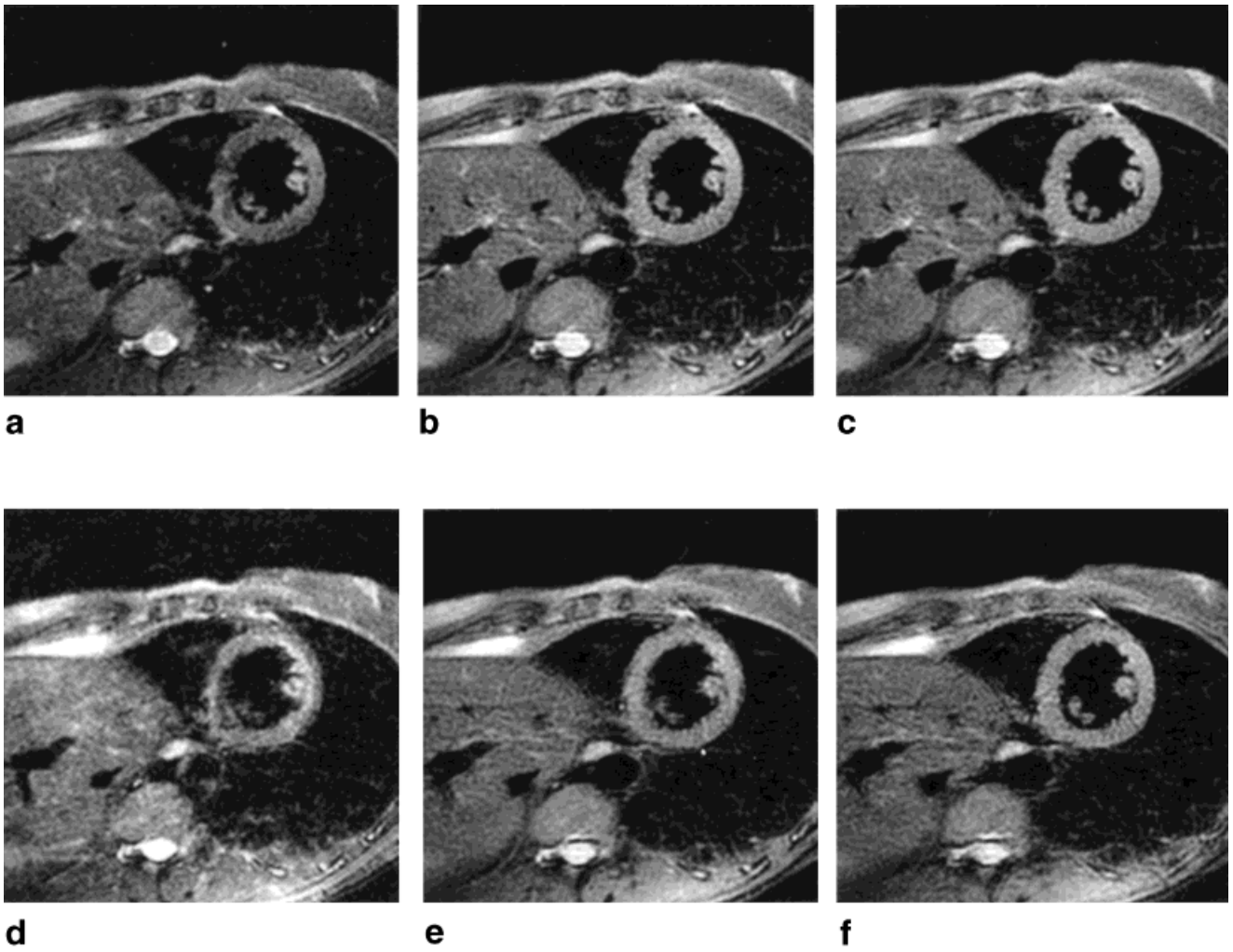

FIG. 6. Short-axis cardiac images with a pseudo-breath-hold (**a–c**) and during free breathing (**d–f**). Images are from (**a,d**) a conventional turbo-spin-echo sequence, (**b,e**) the PROPELLER sequence with no motion correction, and (**c,f**) the PROPELLER sequence with motion correction.

artifact. The author has had difficulties in implementing this as a result of multiple phase pathways that occur during diffusion-weighted turbo-spin-echo sequences, but the work of others (14,15) may remedy this problem.

Extension of the method to three dimensions may be very useful when a volume of image data is desired. This would involve extending the PROPELLER concept from strips to solid rods that rotate in three-dimensional space to form a sphere. The inner sphere of rod overlap could be used to estimate and correct for rotations and shifts in all three directions, eliminating the need for through-plane motion rejection. Correlation weighting would therefore become less important, but could still be used to reduce artifacts attributable to uncorrected (e.g., nonrigid-body) motion.

REFERENCES

1. Glover GH, Pauly JM. Projection reconstruction techniques for reduction of motion effects in MRI. Magn Reson Med 1992;28:275–289.
2. Ahn CB, Kim HH, Cho ZH. High-speed spiral-scan echo planar NMR imaging-I. IEEE Trans Med Imaging 1986;MI-5:2.
3. Meyer CH, Hu BS, Nishimura DG, Macovski A. Fast spiral coronary artery imaging. Magn Reson Med 1992;28:202–213.
4. Nishimura DG, Irarrazabal P, Meyer CH. A velocity *k*-space analysis of flow effects in echo-planar and spiral imaging. Magn Reson Med 1995;33:549–556.
5. Ehman R, Felmlee J. Adaptive technique for high-definition MR imaging of moving structures. Radiology 198;173:255–263.
6. Ordidge RJ, Helpern JA, Qing ZX, Knight RA, Nagesh V. Correction of motional artifacts in diffusion-weighted MR images using navigator echoes. Magn Reson Med 1994;12:455–460.
7. Sachs T, Meyer CH, Irarrazabal P, Hu BS, Nishimura DG, Macouski A. The diminishing variance algorithm for real-time reduction of motion artifacts in MRI. Magn Reson Med 1995;34:412–422.
8. Eddy WF, Fitzgerald M, Noll DC. Improved image registration by using Fourier interpolation. Magn Reson Med 1996;36:923–931.
9. Maas LC, Frederick BD, Renshaw PF. Decoupled automated rotational and translational registration for function MRI time series data: the DART registration algorithm. Magn Reson Med 1997;37:131–139.
10. Jackson JI, Meyer CH, Nishimura DG, Macovski A. Selection of a convolution function for Fourier inversion using gridding. IEEE Trans Med Imaging 1991;10:473–478.
11. Pipe JG, Menon P. Sampling density compensation in MRI: rationale and an iterative numerical solution. Magn Reson Med 1999;41:179–186.

12. Edelman RR, Chien D, Kim D. Fast selective black blood imaging. Radiology 1991;181:655–660.
13. Butts K, Pauly J, deCrespigny A, Mosely M. Isotropic diffusion-weighted and spiral-navigated interleaved EPI for routine imaging of acute stroke. Magn Reson Med 1997;38:741–749.
14. Alsop DC. Phase insensitive preparation of single-shot RARE: application to diffusion imaging in humans. Magn Reson Med 1997;38:527–533.
15. Schick F. SPLICE: Sub-second diffusion-sensitive MR imaging using a modified fast spin-echo acquisition mode. Magn Reson Med 1997;38: 638–644.